Applied Energy 306 (2022) 118037

Contents lists available at ScienceDirect

Applied Energy

journal homepage: www.elsevier.com/locate/apenergy

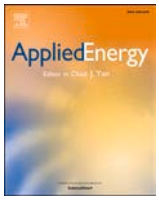

Triboelectric energy harvesting using an origami-inspired structure

Guobiao Hu [a], Chaoyang Zhao [a], Yaowen Yang [a,*], Xin Li [b], Junrui Liang [b,*]

[a] School of Civil and Environmental Engineering, Nanyang Technological University, 50 Nanyang Avenue, 639798 Singapore, Singapore
[b] School of Information Science and Technology, ShanghaiTech University, 393 Middle Huaxia Road, Shanghai 201210, China

HIGHLIGHTS

- Presents a novel Origami triboelectric energy harvester.
- Demonstrates excellent performance of harvester given its stacked architecture.
- Explains effective area enlargement mechanism with a mathematical proof.
- Demonstrates applications of harvester in powering LEDs and an IoT sensor node.

ARTICLE INFO

Keywords:
Triboelectric nanogenerator
Origami
Kinetic energy harvesting
Stacked architecture

ABSTRACT

In this work, the design, fabrication and test of a novel Origami-inspired triboelectric nanogenerator (TENG) are presented. The excellent performance of the proposed Origami-TENG is attributed to its stacked architecture and, thereby, the enlarged effective contact area. The mechanism of effective area enlargement is explained through mathematical proof. The strips used to fabricate the Origami structure are engineered with three layers. For one of the three-layered strips, the top and bottom layers are triboelectric materials with strong negative charge affinities. The middle layer is made of conductive material to constitute the electrode for collecting and guiding the charges induced on the surfaces of the triboelectric materials. The other three-layered conductive strip plays the role of the electrode with a middle polymer layer to provide high flexibility. The performance improvement is validated by the experimental results. Under a periodic tap excitation, the root-mean-square voltage of the proposed Origami-TENG is much larger than that of a conventional counterpart. Moreover, it has been found that by increasing the tapping speed and force, the voltage output from the proposed Origami-TENG can be increased. According to evaluation, the proposed Origami-TENG can produce a power output of around 200 μW. In two application tests, the proposed Origami-TENG can easily light up 28 LEDs and generate sufficient energy in about 40 s to power an electronic device - ViPSN, i.e., a programmable Internet-of-Things sensor node.

1. Introduction

Scavenging energy from the ambient environment to power small electronic devices, such as intelligent wearables, biomechanical implants, and Internet of Things (IoT) network nodes, has attracted enormous attention from the academic and industrial communities [1–3]. The kinetic energy in the form of human motion, ambient vibration and noise, etc., is one of the most ubiquitous energy sources in the environment. Therefore, extensive efforts have been devoted to developing high-efficient energy harvesters for converting mechanical kinetic energy into electrical energy. In general, mechanical-to-electrical energy conversion can be achieved through electromagnetic [4,5], piezoelectric [6–8], electrostatic [9,10], and triboelectric [11–13] transduction mechanisms. In recent years, using triboelectric materials for energy harvesting has received increasing interests, as the raw materials are widely accessible, lightweight, highly flexible, and low-cost.

Since the concept of triboelectric nanogenerator (TENG) was proposed [14], various strategies have been developed to improve TENGs with larger voltage and power outputs [15,16]. From the material perspective, some researchers attempted to modify the material surface at micro- or even nano-scale for achieving strong charge affinities in triboelectric materials [17–21]. Since this paper focuses on the improvement of TENGs brought by structural design, the introduction of material-related research in the literature is not elaborated. From the

* Corresponding authors.
E-mail addresses: cywyang@ntu.edu.sg (Y. Yang), liangjr@shanghaitech.edu.cn (J. Liang).

https://doi.org/10.1016/j.apenergy.2021.118037
Received 10 August 2021; Received in revised form 5 October 2021; Accepted 8 October 2021

structure perspective, innovative TENGs designs with enlarged contact areas have been conceived based on stacked architecture [22,23] and multi-layered structures [24,25]. Though enlarging the effective contact area often significantly increase the power output from TENGs, some stacked/multi-layered structures presented in the literature are bulky and complicated to fabricate.

Origami, which refers to the art of paper folding, has inspired lots of innovative research in different disciplines, ranging from soft robotics [26,27] to programmable metamaterials [28]. In view of the successful applications in these areas, Origami-inspired TENGs have also been developed and reported in recent years. By following a series of pre-designed folding procedures, one can transform a two-dimensional (2D) flat sheet into a compact three-dimensional (3D) Origami structure. Due to the folding operations, the Origami structure is readily multi-layered, which implies an intrinsic advantage and potential for triboelectric energy harvesting. Zhang *et al.* [29] designed a triboelectric harvester based on the Arc pattern Origami tessellation for energy harvesting in road pavement. The Arc pattern Origami tessellation functioned as the base, while the polytetrafluoroethylene (PTFE) and nylon films were pair-wisely attached to the folded facets of the Origami structure. An experimental study validated the feasibility of their proposed Origami-inspired TENG. Tao *et al.* [30] proposed an Origami-inspired electret-based energy harvester. The Origami structure employed by them had a simple double-helix architecture which increased the effective contact area. Moreover, to enhance the electrostatic induction effect, ionized charges were pre-implanted into the film that covered a helix strip of the Origami structure. Xia *et al.* [31] presented an innovative TENG with X-shape by combining the art of cut-paper and Origami-paper. Due to the spatially folded architecture, a power density of 542.2 $\mu W/cm^2$ was achieved.

Due to the lightweight and high flexibility, Origami structures can easily adapt to various forms of human body movements, such as heel strike; ankle, knee, hip, shoulder, and elbow joint motion. Therefore, the Origami-inspired TENGs have a great potential to be used for the application of human motion energy harvesting. However, according to the literature review, the research of using Origami structures for triboelectric energy harvesting is very limited [32–34], despite their great potential in enlarging contact surface area and efficient use of triboelectric materials for significant performance enhancement of TENGs. Though the art of Origami includes more than thousands of folding patterns, the Origami-inspired TENGs reported so far are only based on a few simple folding patterns. The following questions remain unanswered including: Can complex Origami folding patterns be employed in the design of TENGs? How to quantitatively describe and explain the performance enhancement brought by Origami structures? Will Origami-inspired TENGs be able to power practical electronic devices in real applications? To answer these questions, in this work, a novel Origami pattern inspired TENG is investigated. The proposed Origami-TENG can be easily obtained using two continuous flat strips. The interlaced strips can significantly increase the effective contact area during a repeated compress-release process. A physical prototype of the proposed Origami-TENG is fabricated. Experiments are conducted to evaluate its performance. The rest of the paper is organized as follows. The detailed design and fabrication procedures of the proposed Origami-TENG are presented in Section 2. Its working mechanism in terms of performance enhancement is explained in detail. Section 3 includes the experimental results and related discussions. To be more specific, the voltage waveforms, the power level, and application examples are presented. The conclusions of this work are summarized in Section 4.

2. Design and fabrication

This section elaborates the design process of the proposed Origami-inspired TENG and its working principle. A simple TENG generally consists of a pair of contact layers with different charge affinities. Because of the triboelectric effect, static polarized charges could be generated on the surfaces of the tribo-pair layers when they are in contact. The movement of charges takes place under the electrostatic induction effect when the tribo-pair layers are separated by a pair of mechanical forces, thus electricity is produced.

2.1. Material preparation

Though, in principle, materials with different charge affinities can be used to construct the contact pair of a TENG, polymer-based materials are the mostly used because of their advantages, including great flexibility, ease of fabrication, and high cost-effectiveness. According to their material constitution/combination, the tribo-pair layers can be classified into two types of configurations, namely, the polymer–polymer paired configuration and polymer-metal paired configuration. In this study, the polymer-metal paired configuration is adopted just to reduce the cost. The polymer–polymer paired configuration can also be employed in developing a similar Origami-inspired TENG as presented in this work.

The Origami structure for designing the proposed TENG is obtained by repeatedly folding two narrow and long strips. Fig. 1 shows the diagram of the polymer and the electrode strips. The polymer strip (Fig. 1 **(a)**) is formed by stacking two layers of polymer materials and one layer of conductive paper. The polymer materials are used for attaining negative charges. The conductive paper embedded between the two polymer layers servers as the electrode for collecting and guiding the induced charges. It is worth noting that at the two edges along the length direction of the strip, a small portion of polymer materials is intentionally retained. The two edges along the length of the strip are then sealed to avoid a short circuit with the electrode strip that will be introduced below.

The electrode strip (Fig. 1**(b)**) also contains three layers. The top and bottom layers are thin conductive papers. The middle layer is made of polymer material. In fact, one can use pure conductive materials to constitute the electrode strip, and the three-layered architecture is unessential. However, to ease the folding operations in making the Origami structure, the electrode strip is expected to be as flexible as possible. A pure conductive paper can wrinkle easily in an irreversible manner. Therefore, the three-layered electrode strip is used here. The top and bottom conductive layers are thin. The middle layer, composed of polymer material, is used to provide the flexibility of the strip.

In the experiment, polytetrafluoroethylene (PTFE) is selected as the triboelectric material and a conductive cloth tape is used as the electrode strip. More detailed specifications about the two materials will be provided in the later section. Fig. 1**(c) and (d)** show the scanning electron microscope (SEM) images of the surfaces of the two materials after the sputtering process for around 15 min. In Fig. 1**(d)**, one can observe that the surface of the cloth tape appears in a fabric pattern. The fabric pattern of the cloth tape can significantly enhance the ductility while keeping a high conductivity.

2.2. Folding procedures

After the polymer and electrode strips are prepared, we can proceed to construct the Origami structure. The two strips are of the same width. First, the folding lines are determined for a single strip with the given width a. Fig. 2.(a) shows one strip marked with representative folding lines (i.e., the dashed lines). The folding lines for the other strip are exactly the same. α (red) and β (black) are the only two angles needed to determine the folding lines. The distances between the folding lines can be derived as functions of the strip width a as shown in Eq. (1). According to the dimensions of the representative folding lines in Fig. 2.(a), the other folding lines can be recurrently determined. The detailed folding procedures will start from the folding line marked with an arrow symbol.

The parameters illustrated in Fig. 2 can be obtained as follows:

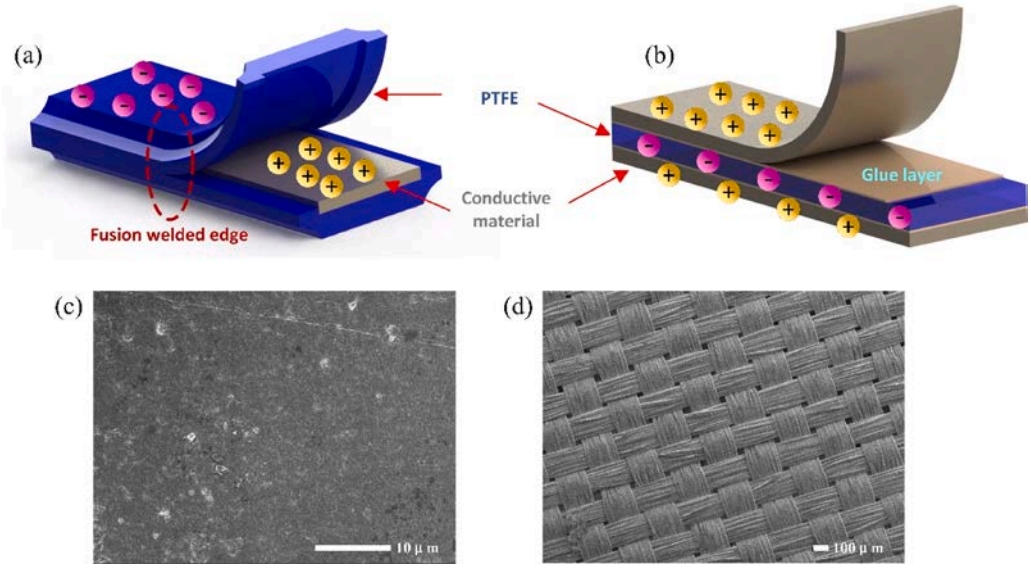

Fig. 1. (a) Three-layer stacked triboelectric strip, (b) double-side conductive electrode strip, (c) SEM image of the PTFE material, (d) SEM image of the conductive fabric material.

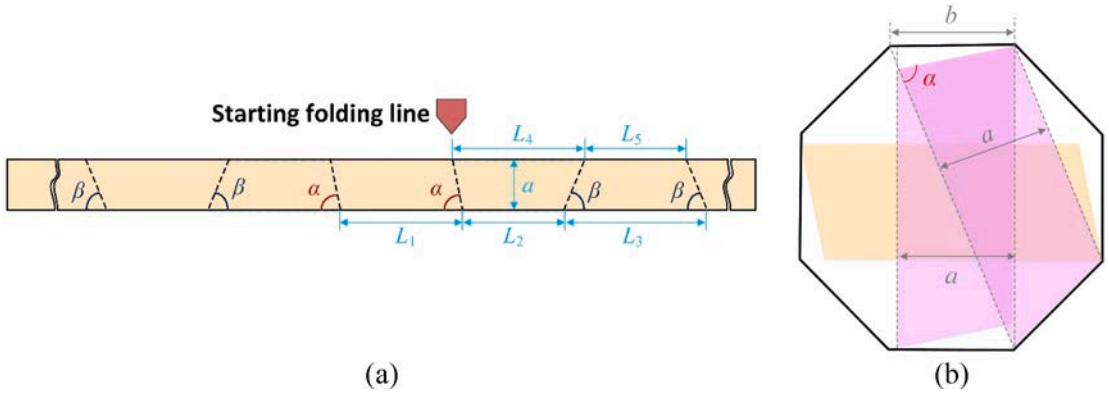

Fig. 2. (a) Representative folding (dashed) lines of a single strip; (b) geometric relationship to determine α.

$$\begin{cases} L_1 = \left(1+\sqrt{2}-cot\alpha\right)b & L_2 = L_5 = 2a \\ L_3 = 2(1+cot\beta)a & L_4 = (2+cot\alpha+cot\beta)a \\ \alpha = 78.75^\circ & \beta = 67.5^\circ \end{cases} \quad (1)$$

where $b = a/sin\beta$. β is half of the internal angle of a regular octagon. α can be determined from the geometric relationship shown in Fig. 2.(b), which demonstrates the bottom layer of the Origami structure. After

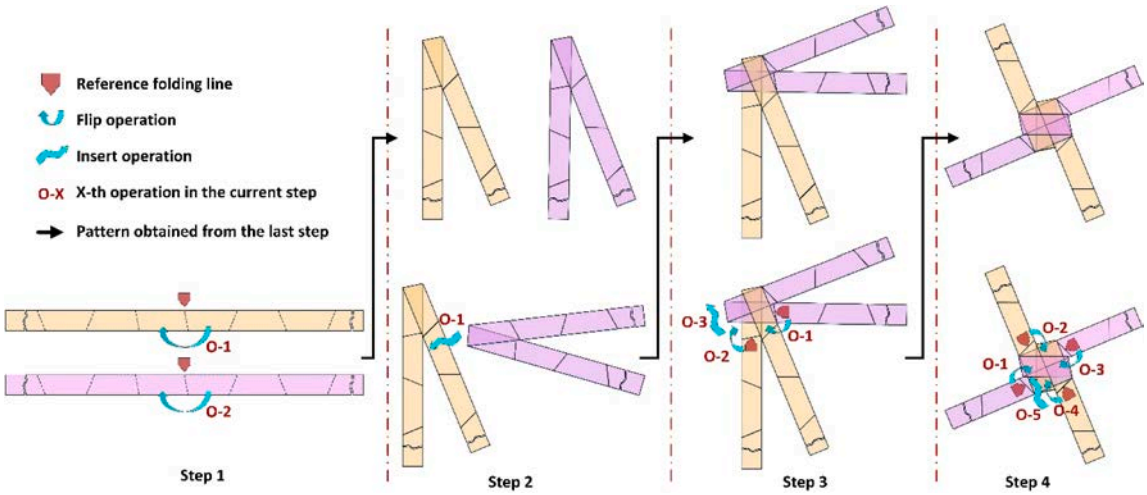

Fig. 3. A step-by-step tutorial for constructing the Origami structure.

determining the folding lines on the strips, we subsequently provide the folding steps, as illustrated in Fig. 3, for constructing the Origami structure. The legend at the left-hand side of the figure explains the symbols that indicate different operations. The orange and violet strips denote the polymer and electrode strips, respectively, or vice versa. Though the instructions only illustrate the first four key steps, one can obtain an Origami structure with arbitrary layers by repeating Step 4. At the end of Step 4, one can find that the top view of the obtained Origami structure is a regular octagon.

According to the folding procedures and the geometric relation shown in Fig. 2, the required length of a single strip to construct this Origami structure with n layers can be calculated as:

$$L_{strip} = \begin{cases} L_1 + (L_2 + L_4) & n = 2 \\ L_1 + (L_2 + L_4) + (n-2)(L_3 + L_5) & n > 2 \end{cases} \tag{2}$$

2.3. Spatial architecture

To help understand the spatial architecture of the obtained Origami structure, Fig. 4 presents its 3D model from different views at different folding stages. By following the Origami design, the two flat strips in the plane form an interlaced and stacked spatial structure, smoothly evolving from 2D to 3D without any cutting or sticking operations. Strip A and Strip B are, respectively, the polymer strip and the electrode strip. Compared to another Origami-based design presented in [35] for which the copper sheets have to be cut into pieces, the fabrication procedures of the current design is much simpler. The electrodes have been well implemented in the material preparation stage. Therefore, the ease of fabrication is one of the advantages of the current design.

Since the strips are made of flexible materials, the Origami structure is easily stretchable in its longitudinal direction. Fig. 4**(e) and (f)**, respectively, present the compressed and stretched states of the Origami structure. Depending on the properties of the raw materials, the obtained Origami structure may behave like a spring with a certain stiffness.

2.4. Working principle

From the fundamental theory of triboelectric harvesting, it is known that the amount of the induced charges, as well as the power output, is proportional to the contact area between the tribo-pair. The Origami structure introduced above has a stacked spatial architecture. The effective contact area between the interlaced strips can be significantly increased, while the cross-sectional area of the Origami structure is still small. Moreover, due to the folding operation, both sides of the polymer/electrode strip can contribute to the increase of the total effective contact area, which profoundly improves the utilization rate of the materials.

Fig. 5 shows the effective areas contributed by the contact between strips within one layer and the contact between strips belonging to two neighbouring layers. Based on the geometric relation illustrated in Fig. 5, one can easily calculate the effective areas:

$$\begin{cases} S_1 = 4a^2 \\ S_2 = b^2 tan\beta + 2b^2 cos^2\beta \end{cases} \tag{3}$$

The cross-sectional area of the regular octagon and the area of the strip segments that constitute one layer are, respectively:

$$\begin{cases} S_{octagon} = 2b^2 tan\beta \\ S_{strip} = 2a(L_3 + L_5) \end{cases} \tag{4}$$

Therefore, we can define the enlargement factor (η_1) of the effective area and the material utilization rate (η_2) as:

$$\begin{cases} \eta_1 = \dfrac{n(S_1 + S_2)}{S_{octagon}} = n\dfrac{sin\beta + 4cos\beta}{2sin\beta} \approx 1.33n \\ \eta_2 = \dfrac{S_1 + S_2}{S_{strip}} = \dfrac{sin\beta + 4cos\beta}{4sin\beta cos\beta(2sin\beta + cos\beta)} \approx 0.78 \end{cases} \tag{5}$$

The enlargement factor (η_1) of the effective area describes the ratio of the total effective contact area to the cross-sectional area of the regular octagon, considering that the thickness of the folded Origami structure is negligible. The material utilization rate (η_2) is mathematically the ratio of the total effective contact area to the one-sided surface area of the strips. The one-sided surface area of the two strips is used because in a conventional dual-plate TENG, only one surface of the two strips contacts with each other. According to the definition, the material utilization rate (η_2) of a conventional dual-plate TENG is 0.5. From Eq. (5), it is learned that with the increase of the number of the stack layers (i.e., n), the effective area enlargement factor (η_1) linearly increases. The material utilization rate (η_2) is a constant, which is larger than 0.5. This is because that both sides of the strips contribute to the total effective area. $\eta_2 > 0.5$ indicates that the stacked architecture demonstrates a much higher material utilization rate than the conventional dual-plate structure.

2.5. Fabricated prototype

In the experiment, for the polymer material, we used polytetrafluoroethylene (PTFE) in view of its strong ability to attain negative charges. The thickness and width of the PTFE film are 0.03 and 50 mm, respectively. In terms of the metal foil, we used double-sided conductive cloth tape. The conductive cloth tape is 35 μm in thickness and dually coated with conductive acrylic adhesive. The width of the cloth tape is 19 mm. Since the PTFE film is wider, we cut it into a narrow strip to adapt to the width of the cloth tape (i.e., approximately 19 mm). Fig. 6 shows the fabricated prototype of the proposed Origami-inspired TENG, which contains 14 layers. Fig. 6**(a) and (b)**, respectively, present the compressed state and the stretched state of the Origami-inspired TENG.

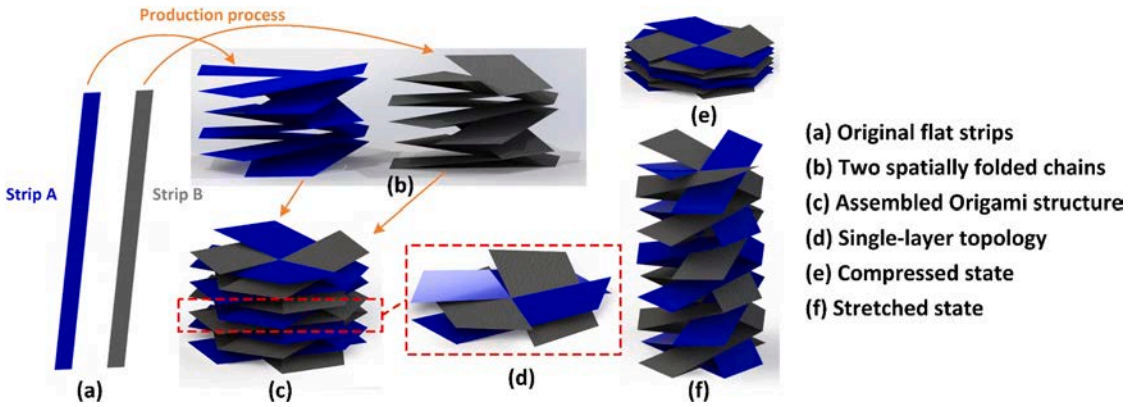

Fig. 4. Demonstration of the spatial architecture of the Origami structure.

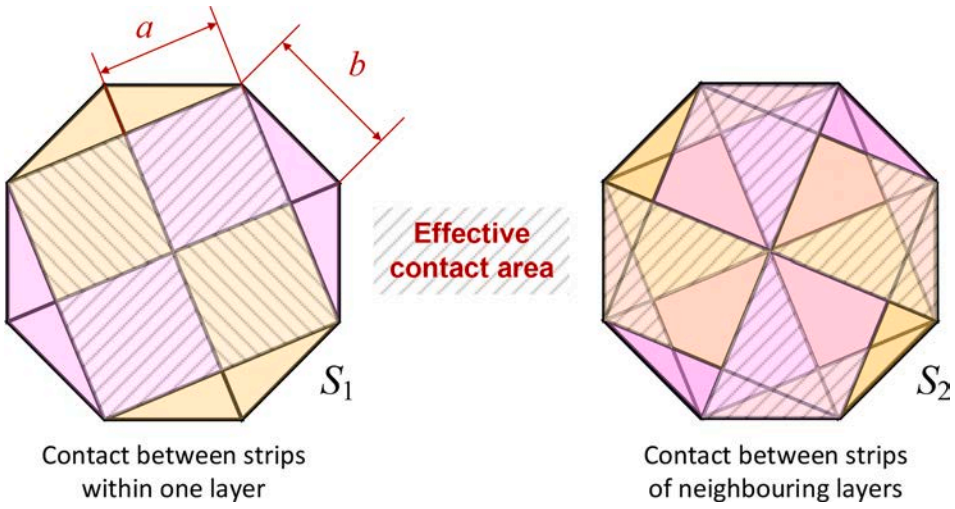

Fig. 5. Effective contact areas between strips within one layer (left) and between strips of neighbouring layers (right).

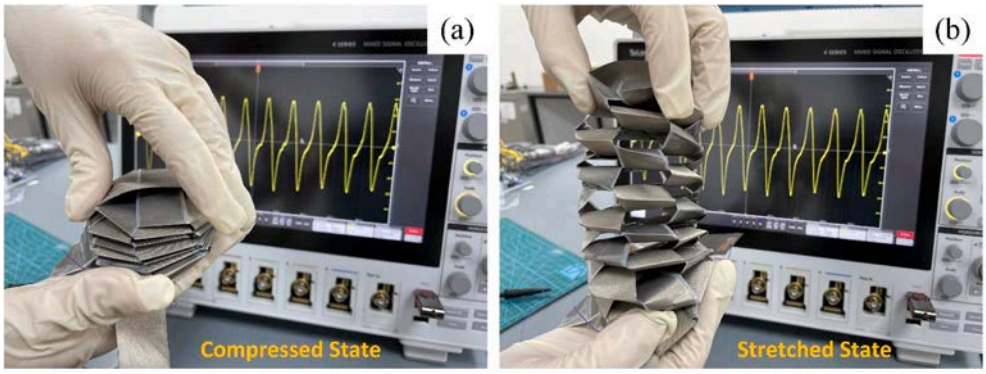

Fig. 6. (a) Compressed and (b) stretched states of the fabricated Origami-inspired TENG.

It can be seen that the obtained Origami structure is flexible and can be easily stretched to a large extent without any damage, implying its high durability and portability. Since the PTFE material itself has a certain elasticity, the surfaces of the layers of the Origami structure at the free state are not completely flat and do not fit each other closely due to the folding process. Thus, the original state of the Origami structure exhibits a certain extent of stiffness. Once we slightly tap the top of the Origami structure, the layers will be compelled to approach each other

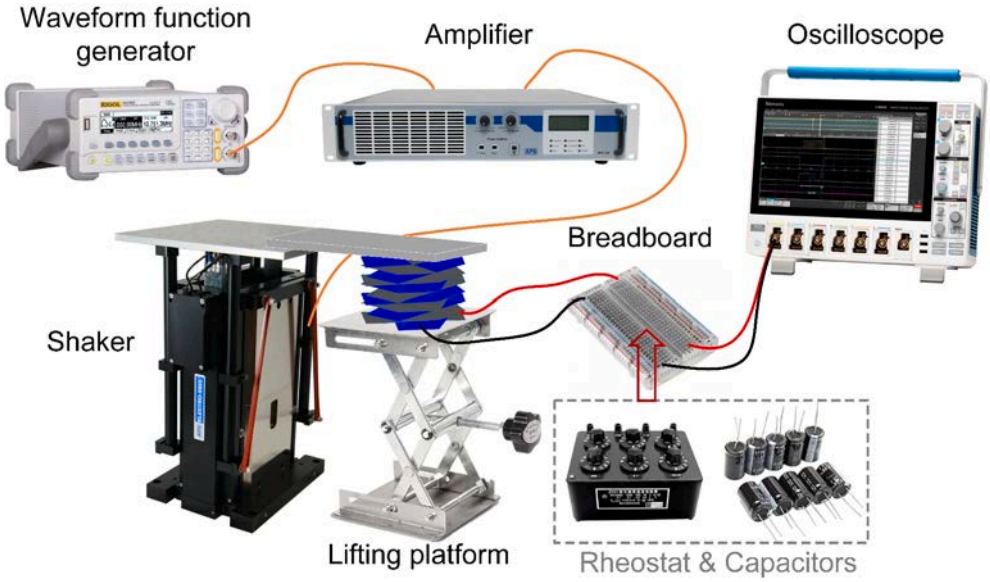

Fig. 7. Experimental setup for testing the Origami-inspired TENG.

and contacts occur between the layers. After releasing the tapping force, the Origami structure will automatically restore to its original state like a spring. Therefore, we can simply tap periodically the top of the Origami structure to induce contact-separation movement between the layers in the experimental test.

3. Experimental setup

The experimental setup shown in Fig. 7 has been prepared for testing the Origami-inspired TENG. A waveform function generator (RIGOL DG1022) is used to generate an excitation signal. The excitation signal is amplified by an amplifier (APS 125), which then drives a shaker (APS 400) to vibrate with desired frequency and amplitude. The Origami-inspired TENG is placed on a lifting platform. A rigid plank is mounted on the top of the shaker, which is used to transfer the vibration from the shaker to the TENG. The gap between the top of the lifting platform and the bottom of the plank can be adjusted. In the experiment, the initial gap is set to be 8 mm, which is the height of the Origami-inspired TENG under the compressed state. The heights of the Origami-inspired TENG under the free state and the stretched state are, respectively, around 15 mm and 25 mm. The Origami-inspired TENG is shunted to a breadboard that holds various electronic elements. An oscilloscope (Tektronix MSO46) is used to measure and record the voltage output from the fabricated Origami-inspired TENG. In the experiment, the gain of the amplifier is tuned to the maximum. The voltage (peak-to-peak) amplitude V_{pp} of the excitation signal generated by the waveform function generator is controlled to change the excitation level. The peak accelerations of the shaker under the control of different input voltages and frequencies are listed in Table 1. Two excitation levels corresponding to $V_{pp} = 10$ V and $V_{pp} = 5$ V are, respectively, referred to as the excitation level $\times$ 2 and $\times$ 1 for conciseness hereinafter.

4. Results and discussion

4.1. Voltage response waveforms

As aforementioned that in principle, the Origami-inspired TENG can produce a considerable output by simply tapping its top, the results from a relatively arbitrary experiment are first presented in prior to the results obtained from the regulated shaker vibration experiment using the facilities shown in Fig. 7. A conventional dual-plate triboelectric harvester [13] that is constituted by a pair of polymer-metal contact surfaces has also been tested for comparison. Fig. 8 presents the voltage responses of the conventional triboelectric harvester and the fabricated Origami-inspired TENG under different tapping conditions.

To obtain the results presented in Fig. 8**(a) and (b)**, we tried to apply periodic taps with almost the same frequency and force. From Fig. 8**(a)**, it is observed that though the maximum voltage amplitude of the conventional TENG is comparable to that of the Origami-inspired one (i.e., Fig. 8**(b)**), the peaks are quite sharp and narrow, resulting in a root-mean-square (RMS) voltage of only 9.38 V. The enveloped area (marked in orange) of the voltage response curve provides a more intuitive graphical explanation. Under the same tapping condition, the RMS voltage output of the Origami-inspired TENG is much larger (i.e., 24.22 V). Subsequently, we increased the tapping force while keeping the same tapping frequency (i.e., the tapping speed). Fig. 8**(c)** shows the corresponding voltage response produced by the Origami-inspired TENG, where the RMS voltage is significantly increased to 48.87 V. Since the increase of the tapping force implies an increased input energy, the above result is easily understandable. Finally, we keep the same tapping force while increase the tapping frequency. From Fig. 8**(d)**, it can be found that the increase of the tapping frequency also enhances the RMS voltage output from the Origami-inspired TENG. Therefore, we can conclude that a faster tapping speed and a stronger tapping force can improve the energy harvesting performance of the Origami-inspired TENG.

Table 1
The peak accelerations of the shaker under the control of different input voltages and frequencies. The values with the unit of g in the table body are the corresponding peak accelerations. g is the gravitational constant.

Control voltage (V)	Frequency (Hz)					
	5	6	7	8	9	10
5 – Level $\times$ 1	0.72 g	0.7 g	0.67 g	0.62 g	0.57 g	0.52 g
10 – Level $\times$ 2	1.44 g	1.4 g	1.34 g	1.24 g	1.14 g	1.04 g

Fig. 9 shows the experimental results under the shaker vibration test using the facilities shown in Fig. 7. The time-history responses exhibit better periodicity, because of the accurate and stable control of the excitation condition. When the excitation frequency is set to be 5 Hz, five repeated cycles appear in the one-second period in Fig. 9**(a) and (b)**. When the excitation is increased to 9 Hz, nine repeated cycles can be identified in the one-second period in Fig. 9**(c)**. Given the excitation frequency of 5 Hz and the excitation level of $\times$ 1, the RMS voltage output from the Origami-inspired TENG is about 23.17 V as demonstrated in Fig. 9**(a)**. When the excitation level is increased to $\times$ 2, the RMS voltage output is increased to 29.15 V as shown in Fig. 9**(b)**. If the excitation level is not increased and still remains at $\times$ 1, while the excitation frequency is increased to 9 Hz, the result presented in Fig. 9**(c)** indicates that the RMS voltage output from the Origami-inspired TENG is also increased to about 30.12 V. It is easy to understand that a higher excitation frequency corresponds to a faster tapping speed, and a higher excitation level corresponds to the tapping condition with a stronger force. Therefore, the experimental results of the shaker vibration test agree with the previous conclusion that increasing the excitation frequency (tapping speed) and level (tapping force) can increase the RMS voltage output from the Origami-inspired TENG.

To ascertain the effects of the excitation level and frequency on the RMS voltage output from the Origami-inspired TENG, Fig. 10**(a)** further presents the results over a wider frequency range. It can be clearly noted that over the low-frequency region, increasing the excitation frequency can increase the RMS voltage output from the Origami-inspired TENG. However, when the excitation frequency is larger than 9 Hz, a further increase of the excitation frequency reduces the RMS voltage output from the Origami-inspired TENG. This could be attributed to that at a higher excitation frequency, the contact period between the layers of the Origami-inspired TENG becomes shorter, and the triboelectric effect is deteriorated. The results under the two different excitation levels are also compared in Fig. 10**(a)**. It is found that increasing the excitation level can always increase the RMS voltage output from the Origami-inspired TENG. Fig. 10**(b)** shows the time-history voltage response from the Origami-inspired TENG at the excitation frequency of 9 Hz and the excitation level $\times$ 2, which corresponds to the condition that the TENG generates the maximum output.

4.2. Power level evaluation

Subsequently, the performance of the Origami-inspired TENG is evaluated in a test of charging capacitors. For three capacitors of different values (i.e., 4.7, 47, and 100 μF), Fig. 11**(a)** shows the time history of the charging voltages. It is noted that for the capacitor of 4.7 μF, the charging voltage quickly increases and reaches quasi-steady in about 30 s. The saturation voltage of the capacitor of 4.7 μF is about 7.1 V under this tapping condition. It will be shown later that by increasing the tapping speed, the saturation voltage can be increased. Under the same tapping condition, it is clear that with the increase of the capacitance, the charging speed decreases. The voltage of the 47 μF capacitor reaches steady (i.e., about 6.3 V) after almost 100 s. However, the 100 μF capacitor still has not reached steady even after 120 s, and the voltage is only about 4.9 V. In Fig. 11**(b)**, for the capacitor of 47 μF, the effect of the tapping speed on the charging rate is investigated. It is evident that with the increase of the tapping speed, the charging rate increases.

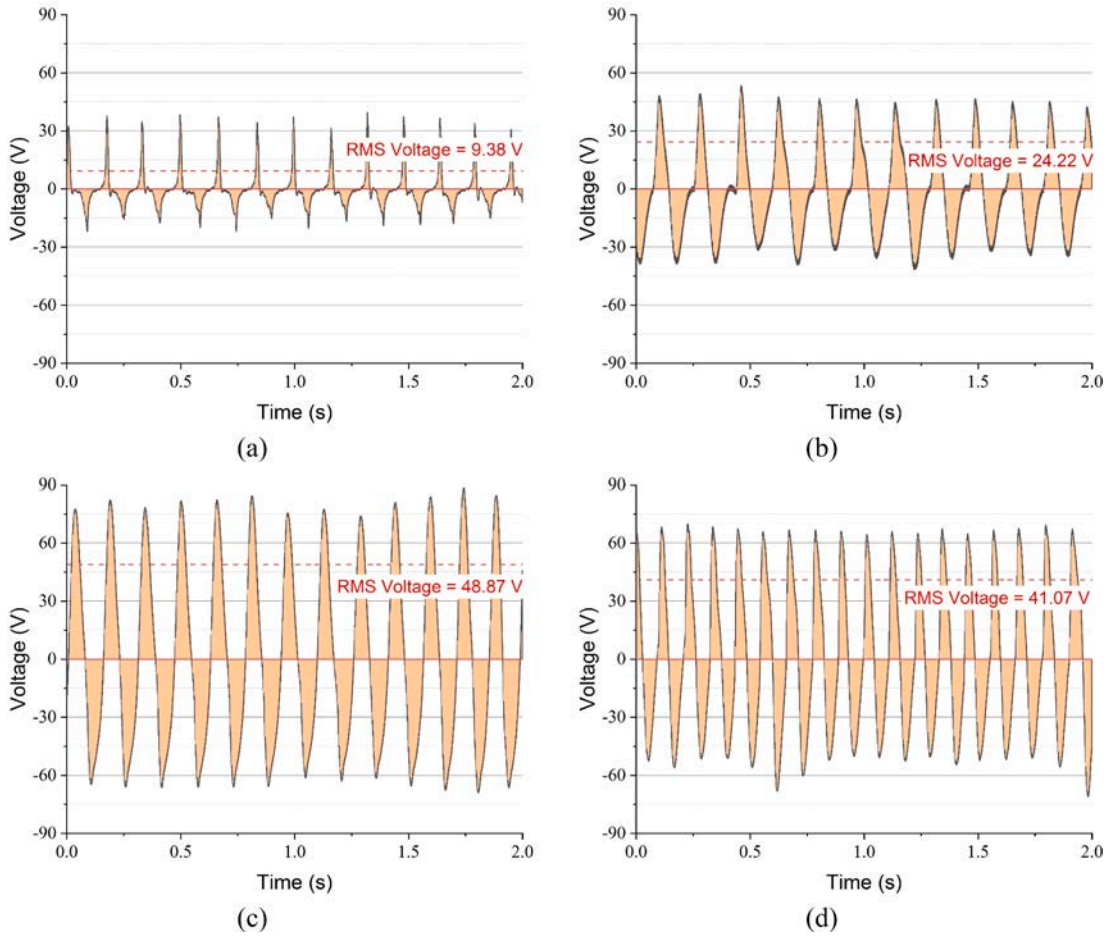

Fig. 8. Voltage responses of (a) a conventional dual-plate TENG under a nearly constant tapping condition, (b) the fabricated Origami-inspired TENG under the almost same tapping condition, (c) the fabricated Origami-inspired TENG under a tapping condition with the almost same frequency but a stronger force, (d) the fabricated Origami-inspired TENG under a tapping condition with the almost same force but a higher frequency.

Moreover, according to the evolution trends of the two curves, it is predictable that a faster tapping speed will possibly lead to a higher saturation voltage. This can be explained by the conclusion obtained from the comparison of Fig. 8**(b) and (d)** that increasing the tapping speed can improve the energy harvesting performance (i.e., a higher voltage output) of the Origami-inspired TENG.

Fig. 12 presents the capacitor charging test results obtained from the regulated experiment. The charging curves are smooth, and the steady voltages (e.g., the case of 9 Hz-×2-4.7μF) are stable. For the capacitor of 4.7μF with a smaller storage capacity, it can be quickly charged to the steady voltage. Given the excitation frequency of 9 Hz and the excitation level of × 2, the capacitor of 4.7μF reaches the steady voltage of 8.45 V in just 24 s. Overall speaking, the results are in good agreement with the previous results obtained from the relatively arbitrary test using hand tapping as the excitation: increasing either the excitation frequency or the excitation level can lead to the increase of the charging speed and the steady voltage.

The power level is an important figure of merit to indicate the capability of an energy harvester. Thus, by shunting the Origami-inspired TENG to different resistances, the power outputs are calculated and presented in Fig. 13. The optimal resistance of a TENG is often at the level of MΩ. Hence, we varied the shunted resistance in the range from 2 to 16 MΩ. As the oscilloscope has a comparable internal resistance of 10 MΩ, the horizontal axis denotes the actual resistance in the measurement. With the increase of the resistance over the investigated range, the power output first increases then decreases. It can be observed that when the shunted resistance is 10 MΩ, the Origami-inspired TENG attains the maximum power output of 189.25 μW. Therefore, the optimal resistance is around 5 MΩ. In fact, the power output also depends on the tapping condition, i.e., the tapping force and speed. The results presented in Fig. 13 at least provide an insight into the approximate power level of the fabricated Origami-inspired TENG.

The results of power output from the Origami-inspired TENG shunted to various resistances under the regulated test are presented in Fig. 14**(a)**. Similarly, the shunted resistance is varied over the range from 2 to 16 MΩ. Noting that the oscilloscope has a comparable internal resistance of 10 MΩ, the horizontal axis denotes the actual resistance. Different from the results presented in Fig. 13, the maximum power output of 193.73 μW is attained when the shunted resistance is 6 MΩ. It indicates that the optimal resistance is about 3.75 MΩ. Compared to the relatively arbitrary test by hand tapping, the maximum power achieved in the regulated experiment is almost the same, which confirms that the power generation capacity of the Origami-inspired TENG is at the level of 200 μW. The cross-section area of the Origami-inspired TENG is a bit smaller than 25 cm^2. Thus, the power density is calculated to be about 77.49 mW/m^2, which is much larger than that of the previous design reported in [35]. The discrepancy in the predictions of the optimal resistance may be caused by two factors. First, the results obtained in the relatively arbitrary test are not sufficiently accurate, since controlling the tapping excitation at the almost same condition by human hands is difficult. Second, under different excitation conditions, the optimal resistance may actually vary. Nonetheless, both results indicate that the optimal resistance should be sought at the level at several MΩ.

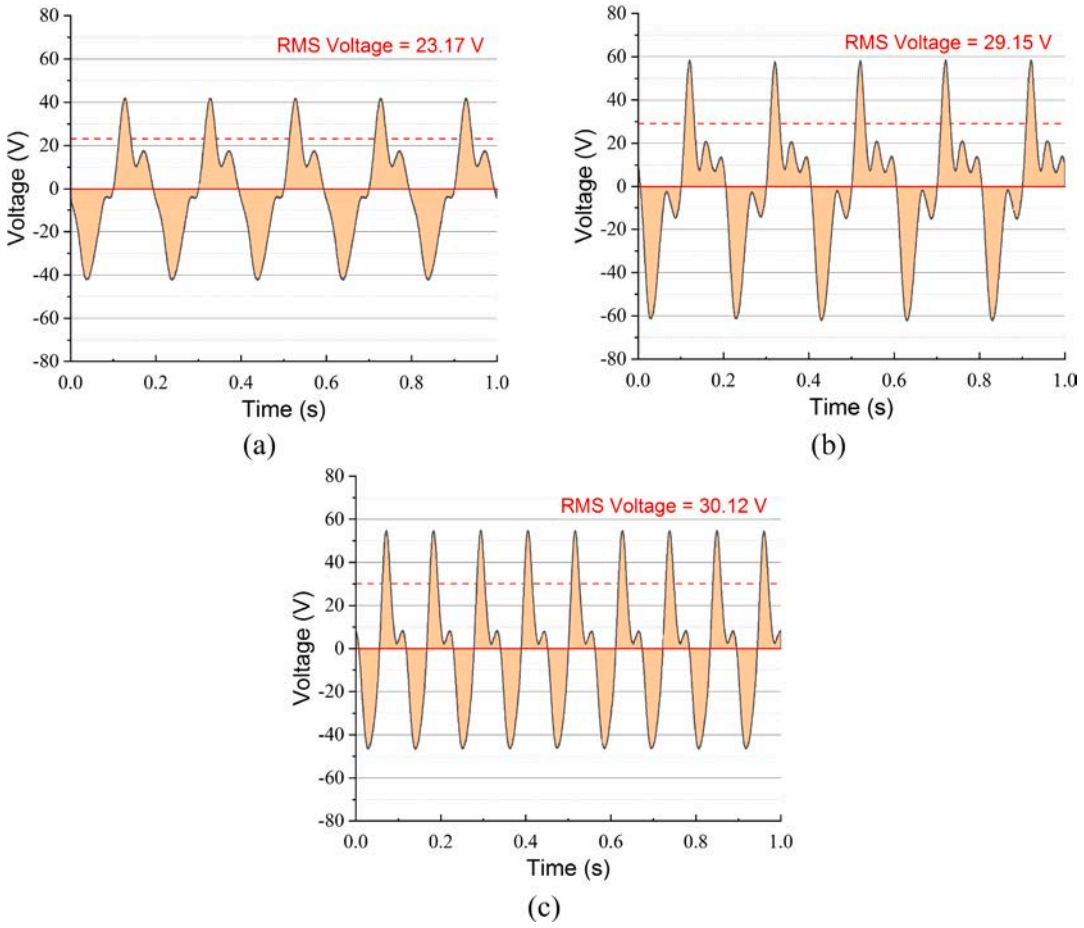

Fig. 9. Voltage responses of the Origami-inspired TENG under the regulated experimental test: (a) the excitation frequency is 5 Hz, and the excitation level is X1; (b) the excitation frequency is 5 Hz, and the excitation level is × 2; (c) the excitation frequency is 9 Hz, and the excitation level is × 1.

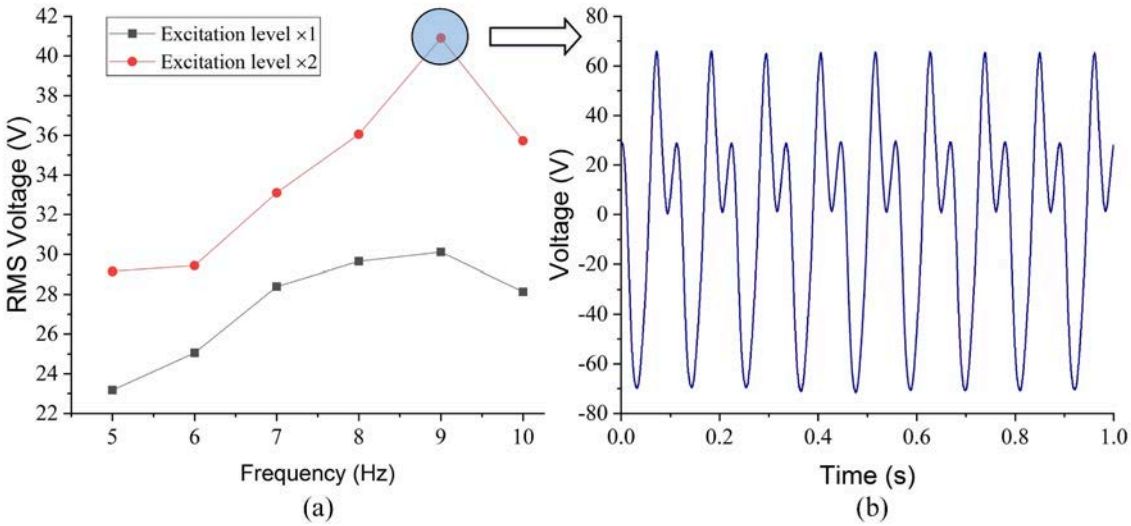

Fig. 10. (a) The RMS voltage from the Origami-inspired TENG versus the excitation frequency; (b) the time-history voltage response from the Origami-inspired TENG at the optimal excitation conditions.

4.3. Practical applications

In addition to estimating the power level, we used the Origami-inspired TENG to power some LEDs and an IoT device. As shown at the bottom of Fig. 15**, 28** LEDs are plugged into a breadboard and connected in series. The forward voltage of a single LED is 3 V. A diode bridge is implemented to convert the alternating-current (AC) output from the Origami-inspired TENG into a direct-current (DC) output. By periodically tapping the Origami-inspired TENG, these 28 LEDs can be lighted up. A video of this demo experiment can be found in the

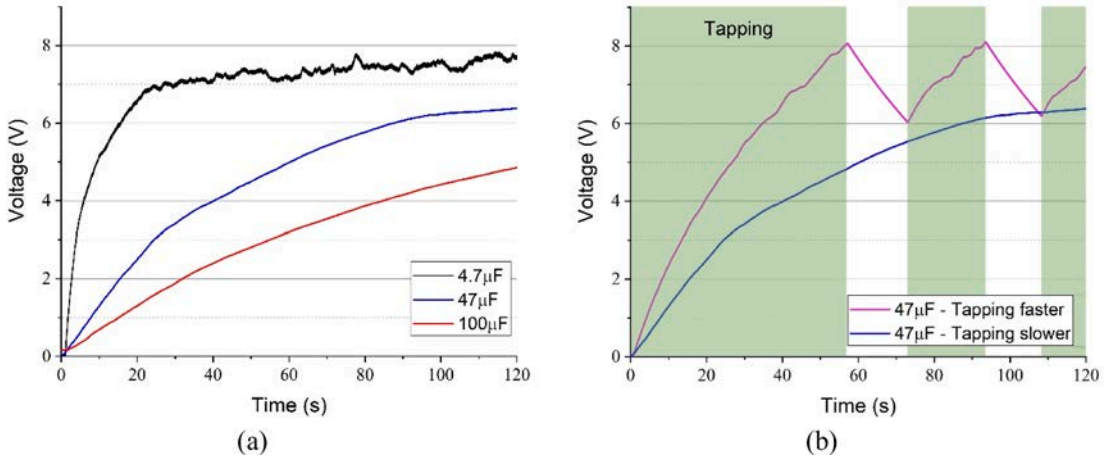

Fig. 11. (a) Charging rates of three different capacitors under the almost same tapping condition, (b) Charging rates of the same capacitor under different tapping speeds.

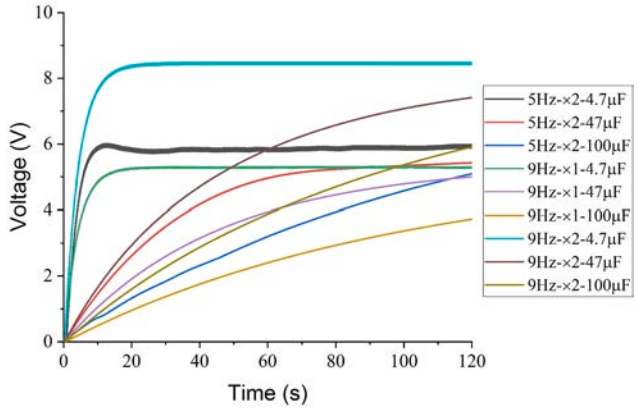

Fig. 12. Charging rates of three different capacitors under different excitation conditions in the regulated experiment test. The legend indicates the excitation condition of each case. For example, 5 Hz-×1-4.7μF means that the excitation frequency is 5 Hz; the excitation level is × 1; and the charging capacitor is 4.7μF.

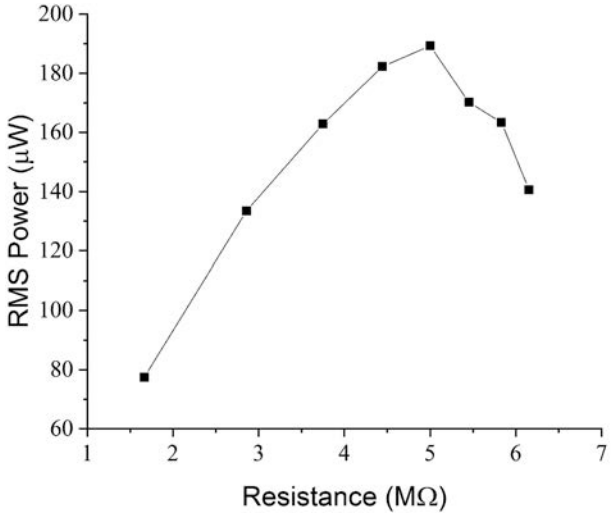

Fig. 13. Power output of the Origami-inspired TENG shunted to various resistances under the test by hand tapping controlled at the almost same condition.

supplementary material S1. Since the tapping by hand could not power the LEDs continuously, they blink according to the pace of tapping. With the increase of the tapping speed, the blinking speed becomes faster.

We also used the Origami-inspired TENG to power an IoT device, i.e., ViPSN [36]. The ViPSN, as shown in Fig. 16**(a)**, is a programmable Internet-of-Things platform that consists of multiple replaceable modules and a motherboard. In the experiment, we selected three modules, namely EEU, EMU, and EUU, and plugged them into the motherboard. The EEU module is constituted by a rectification bridge to achieve AC-DC conversion. The EMU module is the energy management unit, which is composed of functional parts: 1) a DC-DC buck converter; 2) a capacitor of 47 μF for energy storage; and 3) a comparator with adjustable hysteresis. The threshold voltage of the EMU is set to be 5 V in this experiment. Once the voltage of the energy store capacitor exceeds 5 V, implying it has accumulated sufficient energy, the EMU module will start to provide the power supply to the EUU module and trigger it to operate. The EUU module is a node that can carry out temperature sensing and transmit the data via Bluetooth to a connected mobile APP. For the whole charging process, from tapping the Origami TENG till the ViPSN being triggered and the temperature information being sent to a mobile APP, one can refer to the video enclosed in the supplementary material S2. Fig. 16**(b)** shows the photograph of the whole setup at the moment when the mobile APP successfully receives the temperature information from the EUU. In the video, one can note that it takes about 70 s to charge sufficient energy before the EUU module of the ViPSN can operate, i.e., temperature sensing and message transmission. As discussed previously, increasing the tapping force and speed will reduce the time of producing the essential energy for the ViPSN.

In another test, we periodically tap the Origami-inspired TENG with a faster speed (approximately 8 ∼ 9 Hz). Fig. 17 shows the time history of the voltage across the energy storage capacitor of the ViPSN. It is observed that after 39 s, the EUU module is triggered on and a message containing the temperature information is sent to the mobile APP. The triggering voltage is 5 V, which has been programmed in advance. At the end of the sensing and transmission task, the voltage across the energy storage capacitor instantaneously drops to about 3.92 V. We repeated the above process four times, which is reflected by the ups and downs in the time history of the voltage in Fig. 17. Using the formula for calculating the energy stored in a capacitor, i.e., $(1/2)C_r\left(V_{thred}^2 - V_b^2\right)$, we can easily estimate the energy consumed by the ViPSN to complete one task, which is approximately 0.23 mJ. In other words, under the tapping condition in the test, the Origami-inspired TENG can produce more than 0.23 mJ (there is energy loss in other units) in less than 16 s.

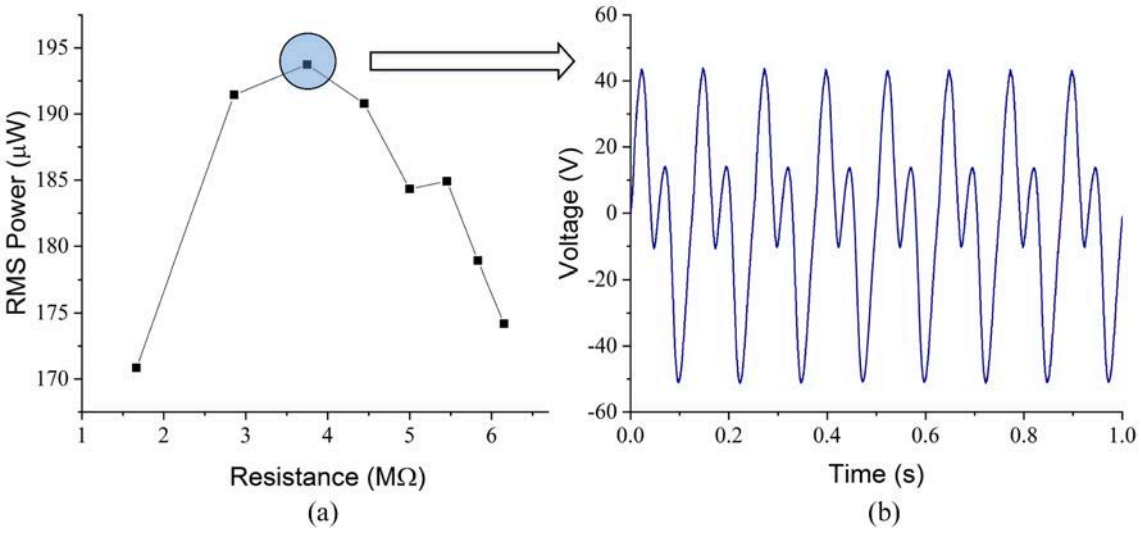

Fig. 14. (a) Power output of the Origami-inspired TENG shunted to various resistances under the regulated test with the excitation frequency of 9 Hz and the excitation level of × 2; (b) the time-history voltage response from the Origami-inspired TENG at the optimal resistance.

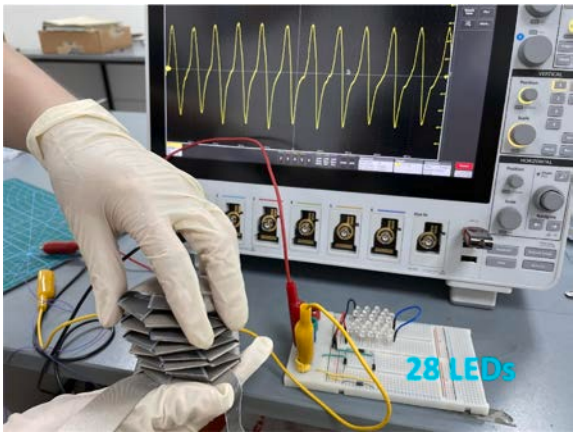

Fig. 15. Demonstration of using the fabricated Origami-inspired TENG to power 28 LEDs connected in series.

5. Conclusions

A novel Origami-inspired TENG has been designed and prototyped. The working principle, especially the effective contact area enlargement due to the stacked architecture of the Origami structure, has been explained. The proposed Origami-TENG has demonstrated an excellent performance in the experimental test. By periodically tapping the top of the proposed Origami-TENG at about 6 Hz, it can easily produce an RMS voltage of more than 20 V. The power level of the proposed Origami-TENG has been evaluated to be around 200 μW. Moreover, a simple parametric study has shown that the power output from the proposed Origami-TENG can be further enhanced by increasing the tapping speed and force. In addition, two practical applications have been demonstrated. In the first application, the proposed Origami-TENG easily lighted up 28 LEDs. In the other application, it produced sufficient energy in around 40 s and successfully powered an electronic device to conduct temperature sensing and standard Bluetooth wireless transmission.

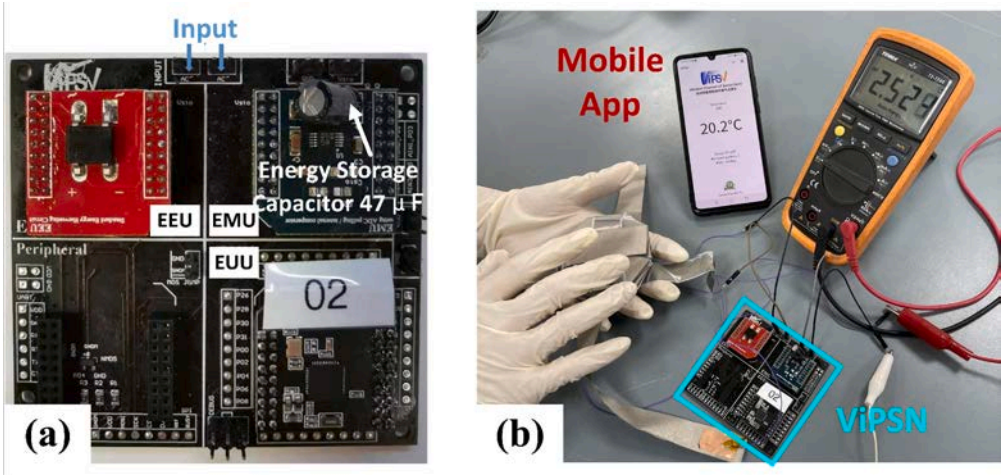

Fig. 16. (a) The motherboard of ViPSN, which is a programmable Internet-of-Things (IoT) platform, with three modules plugged in. The three modules are, respectively, the energy rectification unit – EEU, the energy management unit – EMU, and the energy user unit – EUU. (b) Demonstration of using the fabricated Origami-inspired TENG to power ViPSN.

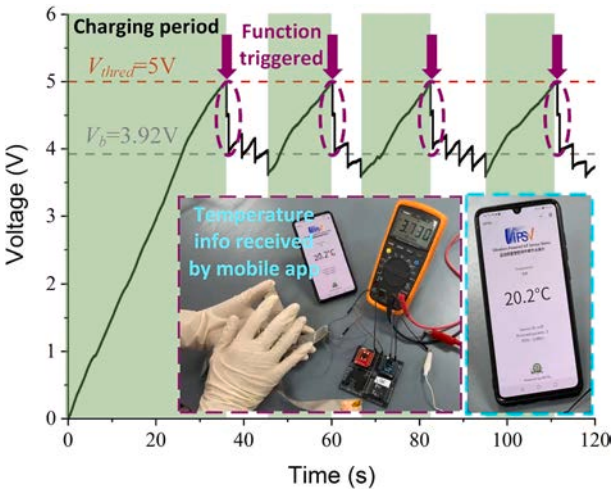

Fig. 17. Time history of the voltage across the energy storage capacitor of the ViPSN when being charged by the Origami-inspired TENG. The light green colour shaded area denotes the charging period, i.e., tapping is applied by hand.

CRediT authorship contribution statement

Guobiao Hu: Conceptualization, Methodology, Software, Investigation, Formal analysis, Writing – original draft. **Chaoyang Zhao:** Methodology, Investigation, Formal analysis. **Yaowen Yang:** Investigation, Project administration, Writing – review & editing, Resources, Supervision. **Xin Li:** Investigation, Methodology. **Junrui Liang:** Investigation, Writing – review & editing, Supervision.

Declaration of Competing Interest

The authors declare that they have no known competing financial interests or personal relationships that could have appeared to influence the work reported in this paper.

Appendix A. Supplementary data

Supplementary data to this article can be found online at https://doi.org/10.1016/j.apenergy.2021.118037.

References

[1] Kamalinejad P, Mahapatra C, Sheng Z, Mirabbasi S, Leung VC, Guan YL. Wireless energy harvesting for the Internet of Things. IEEE Commun Mag 2015;53(6):102–8.
[2] Shaikh FK, Zeadally S. Energy harvesting in wireless sensor networks: A comprehensive review. Renew Sustain Energy Rev 2016;55:1041–54.
[3] Liu L, Guo X, Lee C. Promoting smart cities into the 5G era with multi-field Internet of Things (IoT) applications powered with advanced mechanical energy harvesters. Nano Energy 2021:106304.
[4] Li Z, Yan Z, Luo J, Yang Z. Performance comparison of electromagnetic energy harvesters based on magnet arrays of alternating polarity and configuration. Energy Convers Manage 2019;179:132–40.
[5] Elvin NG, Elvin AA. An experimentally validated electromagnetic energy harvester. J Sound Vib 2011;330(10):2314–24.
[6] Fang S, Wang S, Zhou S, Yang Z, Liao W-H. Exploiting the advantages of the centrifugal softening effect in rotational impact energy harvesting. Appl Phys Lett 2020;116(6):063903.
[7] Wang J, Zhou S, Zhang Z, Yurchenko D. High-performance piezoelectric wind energy harvester with Y-shaped attachments. Energy Convers Manag 2019;181:645–52.
[8] Zhou S, Cao J, Inman DJ, Lin J, Liu S, Wang Z. Broadband tristable energy harvester: modeling and experiment verification. Appl Energy 2014;133:33–9.
[9] Hoffmann D, Folkmer B, Manoli Y. Analysis and characterization of triangular electrode structures for electrostatic energy harvesting. J Micromech Microeng 2011;21(10):104002.
[10] Tao K, Lye SW, Miao J, Hu X. Design and implementation of an out-of-plane electrostatic vibration energy harvester with dual-charged electret plates. Microelectron Eng 2015;135:32–7.
[11] Khandelwal G, Chandrasekhar A, Alluri NR, Vivekananthan V, Raj NPMJ, Kim S-J. Trash to energy: A facile, robust and cheap approach for mitigating environment pollutant using household triboelectric nanogenerator. Appl Energy 2018;219:338–49.
[12] Rahman MT, Rana SS, Salauddin M, Maharjan P, Bhatta T, Kim H, et al. A highly miniaturized freestanding kinetic-impact-based non-resonant hybridized electromagnetic-triboelectric nanogenerator for human induced vibrations harvesting. Appl Energy 2020;279:115799.
[13] Zhao C, Yang Y, Upadrashta D, Zhao L. Design, modeling and experimental validation of a low-frequency cantilever triboelectric energy harvester. Energy 2021;214:118885.
[14] Fan F-R, Tian Z-Q, Wang ZL. Flexible triboelectric generator. Nano Energy 2012;1(2):328–34.
[15] Guo X, Liu L, Zhang Z, Gao S, He T, Shi Q, et al. Technology evolution from micro-scale energy harvesters to nanogenerators. J Micromech Microeng 2021;31:093002.
[16] Zhu J, Zhu M, Shi Q, Wen F, Liu L, Dong B, et al. Progress in TENG technology—A journey from energy harvesting to nanoenergy and nanosystem. EcoMat 2020;2(4):e12058.
[17] Cheng X, Song Z, Miao L, Guo H, Su Z, Song Y, et al. Wide range fabrication of wrinkle patterns for maximizing surface charge density of a triboelectric nanogenerator. J Microelectromech Syst 2017;27(1):106–12.
[18] Parajuli P, Sharma B, Behlow H, Rao AM. Fullerene-Enhanced Triboelectric Nanogenerators. Advanced Materials Technologies 2020;5(8):2000295.
[19] Wang J, Wu C, Dai Y, Zhao Z, Wang A, Zhang T, et al. Achieving ultrahigh triboelectric charge density for efficient energy harvesting. Nat Commun 2017;8(1):1–8.
[20] Rasel MSU, Park J-Y. A sandpaper assisted micro-structured polydimethylsiloxane fabrication for human skin based triboelectric energy harvesting application. Appl Energy 2017;206:150–8.
[21] Li S, Nie J, Shi Y, Tao X, Wang F, Tian J, et al. Contributions of different functional groups to contact electrification of polymers. Adv Mater 2020;32(25):2001307.
[22] Yang W, Chen J, Jing Q, Yang J, Wen X, Su Y, et al. 3D stack integrated triboelectric nanogenerator for harvesting vibration energy. Adv Funct Mater 2014;24(26):4090–6.
[23] Gao L, Hu D, Qi M, Gong J, Zhou H, Chen X, et al. A double-helix-structured triboelectric nanogenerator enhanced with positive charge traps for self-powered temperature sensing and smart-home control systems. Nanoscale 2018;10(42):19781–90.
[24] Zhang LM, Han CB, Jiang T, Zhou T, Li XH, Zhang C, et al. Multilayer wavy-structured robust triboelectric nanogenerator for harvesting water wave energy. Nano Energy 2016;22:87–94.
[25] Xu M, Wang P, Wang YC, Zhang SL, Wang AC, Zhang C, et al. A soft and robust spring based triboelectric nanogenerator for harvesting arbitrary directional vibration energy and self-powered vibration sensing. Adv Energy Mater 2018;8(9):1702432.
[26] Rus D, Tolley MT. Design, fabrication and control of origami robots. Nat Rev Mater 2018;3(6):101–12.
[27] Belke CH, Paik J. Mori: a modular origami robot. IEEE/ASME Trans Mechatron 2017;22(5):2153–64.
[28] Silverberg JL, Evans AA, McLeod L, Hayward RC, Hull T, Santangelo CD, et al. Using origami design principles to fold reprogrammable mechanical metamaterials. Science 2014;345(6197):647–50.
[29] Zhang H, Yang C, Yu Y, Zhou Y, Quan L, Dong S, et al. Origami-tessellation-based triboelectric nanogenerator for energy harvesting with application in road pavement. Nano Energy 2020;78:105177.
[30] Tao K, Yi H, Yang Y, Chang H, Wu J, Tang L, et al. Origami-inspired electret-based triboelectric generator for biomechanical and ocean wave energy harvesting. Nano Energy 2020;67:104197.
[31] Xia K, Zhu Z, Zhang H, Du C, Xu Z, Wang R. Painting a high-output triboelectric nanogenerator on paper for harvesting energy from human body motion. Nano Energy 2018;50:571–80.
[32] Wang Y, Wu Y, Liu Q, Wang X, Cao J, Cheng G, et al. Origami triboelectric nanogenerator with double-helical structure for environmental energy harvesting. Energy 2020;212:118462.
[33] Chung J, Song M, Chung S-H, Choi W, Lee S, Lin Z-H, et al. Triangulated Cylinder Origami-Based Piezoelectric/Triboelectric Hybrid Generator to Harvest Coupled Axial and Rotational Motion. Research 2021;2021.
[34] Yang P-K, Lin Z-H, Pradel KC, Lin L, Li X, Wen X, et al. Paper-based origami triboelectric nanogenerators and self-powered pressure sensors. ACS Nano 2015;9(1):901–7.
[35] C. Chen, D. Howard, S.L. Zhang, Y. Do, S. Sun, T. Cheng, Z.L. Wang, G.D. Abowd, and H. Oh. *SPIN (self-powered paper interfaces) bridging triboelectric nanogenerator with folding paper creases*. in *Proceedings of the Fourteenth International Conference on Tangible, Embedded, and Embodied Interaction*. 2020.
[36] Li X, Teng L, Tang H, Chen J, Wang H, Liu Y, et al. ViPSN: A vibration-powered iot platform. IEEE Internet Things J 2020;8(3):1728–39.